Eikonal profile functions and amplitudes for pp and $\bar{p}p$ scattering

Flávio Pereira
Observatório Nacional, CNPq, Rio de Janeiro 20921-400, RJ, Brazil

Erasmo Ferreira
Instituto de Física, Universidade Federal do Rio de Janeiro, Rio de Janeiro 21945-970, RJ, Brazil

(Received 9 June 1998; published 19 November 1998)

The eikonal profile function $J(b)$ obtained from the model of the stochastic vacuum is parametrized in a form suitable for comparison with experiment. The amplitude and the extended profile function (including imaginary and real parts) are determined directly from the complete pp and $\bar{p}p$ elastic scattering data at high energies. A full and accurate representation of the data is presented, with a smooth energy dependence of all parameters. The changes needed in the original profile function required for the description of scattering beyond the forward direction are described. [S0556-2821(98)05523-4]

PACS number(s): 13.85.Dz, 12.40.Nn, 13.85.Lg

I. INTRODUCTION

The application of the model of the stochastic vacuum (MSV) [1–3] to pp and $\bar{p}p$ scattering gives a good description of the experimental quantities related to the amplitude in the forward direction. For large values of the momentum transfer $|t|$ the experimental amplitude has a delicate structure, with a characteristic dip in the differential elastic cross section that is not reproduced by MSV or other dynamical models without free parameters. It is well known that the profile function of the eikonal formalism, related to the amplitude through a two-dimensional Fourier transform, has an apparently structureless shape, and slight changes in the profile may cause dramatic changes in the amplitude. The main reason is that the dominating imaginary part of the amplitude passes through zero for a value of $|t|$ which is not large, while the real part, being comparatively small for low $|t|$, fills partially the dip due to the zero of the imaginary part, thus producing the remarkable structure of the differential cross section. This is not really a shortcoming of MSV, since this model, in its present formulation using the first term of an expansion based on the eikonal formalism, has not the purpose of describing the differential cross section much beyond the $|t|=0$ limit.

Our study of the MSV profile function suggests analytical forms which can be used, with appropriate changes of parameters, to describe the data in the full range of $|t|$ values. In order to identify the necessary changes, we first describe accurately the whole data of high-energy pp [at the CERN Intersecting Storage Rings (ISR) energies $\sqrt{s}=20-60$ GeV] and $\bar{p}p$ (at $\sqrt{s}=540$ and 1800 GeV) scattering in terms of an amplitude built with a few terms controlled by a number of parameters. This part of our work is similar to the treatment of the ISR data by Carvalho and Menon [4], but our parameters are fewer and have a much more regular energy dependence (which is essential to allow for predictions through interpolations and extrapolations). The comparison of the two different parametrizations exhibits some freedom of analytical forms allowed by the data.

The use of an impact picture representation for the scattering amplitude of pp and $\bar{p}p$ scattering was made by Bourrely, Soffer, and Wu [5]. With a t dependence inspired in the proton electromagnetic form factor, using a total of six adjustable parameters, they are able to reproduce the general features of the ISR experiments. The form of the energy dependence is based on general properties of quantum field theory, and has allowed good predictions for the CERN measurements at 540 GeV. The difference of approach with respect to our work is that we take different forms of parametrization (inspired by the model of the stochastic vacuum) and that we do not parametrize the energy dependence. We show that very accurate fitting at every energy can be obtained with very smooth energy dependence for the parameters. Our description includes the data at very high $|t|$ (up to 15 GeV^2) valid for all ISR energies and we remark that the sign of the term describing this tail is reponsible for differences between pp and $\bar{p}p$ data in this range. In the work of Bourrely, Soffer, and Wu this large $|t|$ tail would be described by the Regge background term.

We attempt to obtain from the shapes of the eikonal functions some understanding of the geometric characteristics of the systems in collision, and thus try to visualize from the data the meaning of effective radii for hadrons in collision [6].

Table I shows the available data on total cross sections, slope parameter and ratio of the forward real to imaginary

TABLE I. Experimental data.

	$\sqrt{s}$ (GeV)	σ^T (mb)	B (GeV^2)	Ref. [7]	$\bar{\rho}$	Ref. [7]
	23.5	39.65 ± 0.22	11.80 ± 0.30	*(a)*	0.020 ± 0.050	*(b,c)*
	30.7	40.11 ± 0.17	12.20 ± 0.30	*(a)*	0.042 ± 0.011	*(b,c)*
pp	44.7	41.79 ± 0.16	12.80 ± 0.20	*(b)*	0.062 ± 0.011	*(b,c)*
	52.8	42.38 ± 0.15	12.87 ± 0.14	*(a)*	0.078 ± 0.010	*(b,c)*
	62.5	43.55 ± 0.31	13.02 ± 0.27	*(a)*	0.095 ± 0.011	*(b,c)*
$\bar{p}p$	541	62.20 ± 1.50	15.52 ± 0.07	*(d)*	0.135 ± 0.015	*(d)*
	1800	72.20 ± 2.70	16.72 ± 0.44	*(e)*	0.140 ± 0.069	*(e)*

parts of the amplitude in pp scattering, which come from the CERN Intersecting Storage Rings (ISR) measurements [7a,b,c] at energies ranging from $\sqrt{s}=23$ GeV to $\sqrt{s}=63$ GeV, and in $\bar{p}p$ scattering at the energies $\sqrt{s}=541-546$ GeV from the CERN Super Proton Synchrotron [7d] and the $\sqrt{s}=1800$ GeV information [7e] from Fermilab. In addition, there are the data on differential cross sections in the range $\sqrt{s}=23-63$ GeV [7a,8], and for $\bar{p}p$ at $\sqrt{s}=546$ GeV [9] and $\sqrt{s}=1800$ GeV [10]. We also give particular attention to the behavior of the amplitude for large $|t|$ measured [11] at $\sqrt{s}=27$ GeV. The data from the Collider Detector at Fermilab (CDF) [12] at 1800 GeV giving $\sigma^T=80$ mb seem discrepant when we consider the smoothness of the energy dependence of our parametrization, and also is not in agreement with the predictions of Bourrely, Soffer, and Wu [5], and thus in the present work we concentrate on the results of the Fermilab E-710 experiment given in Table I.

In the MSV calculation hadronic structures enter through transverse two-dimensional wave functions in the plane perpendicular to the direction of the colliding hadrons, for which is made the simple ansatz

$$\psi_H(R)=\sqrt{2/\pi}\frac{1}{S_H}\exp(-R^2/S_H^2), \tag{1}$$

where S_H is a parameter for the hadron size. The dimensionless scattering amplitude $T_{H_1H_2}$ in the eikonal formalism is given in terms of the dimensionless profile function $\hat{J}_{H_1H_2}$ for hadron-hadron scattering by

$$T_{H_1H_2}=is[\langle g^2FF\rangle a^4]^2a^2 \times\int d^2\vec{b}\,\exp(i\vec{q}\cdot\vec{b})\hat{J}_{H_1H_2}(\vec{b},S_1,S_2), \tag{2}$$

where the impact parameter vector $\vec{b}$ and the hadron sizes S_1, S_2 appear only in units of the correlation length a, and $\vec{q}$ is the momentum transfer projected on the transverse plane, in units of $1/a$, so that the momentum transfer squared is $t=-|\vec{q}|^2/a^2$. The quantity $\langle g^2FF\rangle$ represents the gluon condensate. For short, from now on we write $J(b)$ or $J(b/a)$ to represent $\hat{J}_{H_1H_2}(\vec{b},S_1,S_2)$. The normalization of $T_{H_1H_2}$ is such that total and differential cross sections are given by

$$\sigma^T=\frac{1}{s}\,\mathrm{Im}\,T_{H_1H_2},\quad \frac{d\sigma^{el}}{dt}=\frac{1}{16\pi s^2}|T_{H_1H_2}|^2. \tag{3}$$

To write convenient expressions for the observables, we define the dimensionless moments of the profile function (as before, with b in units of the correlation length a)

$$I_k=\int d^2\vec{b}\,b^kJ(b),\quad k=0,1,2,\ldots, \tag{4}$$

which depend only on S_1/a, S_2/a, and the Fourier-Bessel transform

$$I(t)=\int d^2\vec{b}J_0(ba\sqrt{|t|})J(b), \tag{5}$$

where $J_0(ba\sqrt{|t|})$ is the zeroth-order Bessel function. Then

$$T_{H_1H_2}=is[\langle g^2FF\rangle a^4]^2a^2I(t). \tag{6}$$

Since $J(b)$ is real, σ^T and the slope parameter B are written

$$\sigma^T=I_0[\langle g^2FF\rangle a^4]^2a^2,$$

$$B=\frac{d}{dt}\left(\ln\frac{d\sigma^{el}}{dt}\right)\bigg|_{t=0}=\frac{1}{2}\frac{I_2}{I_0}a^2\equiv Ka^2. \tag{7}$$

It is important to observe that these results conveniently factorize the dimensionless QCD strength $\langle g^2FF\rangle a^4$ in the expressions for the amplitude, and that the correlation length a appears as the natural length scale for the observables and for the geometric aspects of the interaction. For forward scattering these aspects are concentrated on the quantities $I_0(S_1/a,S_2/a)$ and $I_2(S_1/a,S_2/a)$ that depend on the hadronic structures and are mainly determined by the values of the profile functions in the range of impact parameter up to about 2.5 fm. The total cross section σ^T measures the strength, while the slope B has the strength cancelled out and is only related to the hadron geometry. The explicit formula for the slope is

$$B=\frac{1}{2}\,\frac{\int d^2\vec{b}b^2J(b)}{\int d^2\vec{b}J(b)}a^2=\frac{1}{2}\langle b^2\rangle a^2, \tag{8}$$

where it is seen as related to the average value of the square of the impact parameter in the collision, with $J(b)$ as the weight function. We recall that here b is dimensionless and that $\langle b^2\rangle$ depends on the hadronic sizes.

The paper is organized as follows. In Sec. II we present a convenient parametrization of the MSV profile function in terms of which the observable quantities are calculated. In Sec. III amplitudes and profile functions are directly obtained from experimental data and comparison is made between our results and those of Carvalho and Menon [4]. In Sec. IV we present general comments and conclusions.

II. MSV PROFILE FUNCTIONS

The analytical study [2] of the MSV profile functions for large values of b shows that their asymptotic behavior is of the form

$$J(b)=\exp(-\rho b)\left[\frac{A_1}{b}+\frac{A_2}{b^2}+\ldots\right], \tag{9}$$

where $A_1,A_2,\ldots$ are functions of S_1/a and S_2/a, and the quantity $\rho=3\pi/8$ arises from the particular form of corrrelation function that has been used. For small and intermedi-

ate values of b the form of $J(b)$ resembles Gaussian shapes, which combined with the results of MSV for large b leads us to suggest the form

$$J(b)=[J(0)-a_3]e^{-b^2/a_1}+a_3e^{-b^2/a_2}+a_4\tilde{A}_\gamma(b), \quad (10)$$

with

$$\tilde{A}_\gamma(b)=\frac{e^{-\rho\sqrt{\gamma^2+b^2}}}{\sqrt{\gamma^2+b^2}}(1-e^{\rho\gamma-\rho\sqrt{\gamma^2+b^2}}). \quad (11)$$

The last term fixes the correct behavior of $J(b)$ for large b given in Eq. (9), with $\sqrt{\gamma^2+b^2}$ written in the place of b, so that the expression can be extended to $b=0$. The combination inside the parentheses is such that $\tilde{A}_\gamma(0)=0$, and it is shown below that the use of the two terms creates a zero in the imaginary part of the amplitude, which is required by the data.

The parameters $a_1, a_2, a_3, a_4, \gamma$ depend on S_1 and S_2. In pp and $\bar{p}p$ scattering we have $S_1=S_2\equiv S$, and the behavior of the parameters as functions of S/a is regular and simple. Good representations are

$$J(0)=\frac{0.0024(S/a)^4}{4.5+(S/a)^3}, \quad (12)$$

$$a_1=10+0.285(S/a)^3, \quad (13)$$

$$a_2=1+0.25(S/a)^2, \quad (14)$$

$$a_3=\frac{0.002745(S/a)^3}{4+(S/a)^2}, \quad (15)$$

$$a_4=\frac{4}{2187\pi^2}[1+e^{(\rho S/2a)^2}]^2(S/a)^4, \quad (16)$$

and

$$\gamma=0.57(S/a)^2. \quad (17)$$

The expression for a_4 shows the fast increase of the thickness of the asymptotic tail as S/a grows. The contributions of the terms in Eq. (10) are illustrated in Fig. 1, together with the profile $J(b)$ obtained by direct calculation [1].

With the analytical expression (10) for $J(b)$, the integrations leading to the moments I_k are easily performed, leading to

$$I_0=2\pi\left(\frac{1}{2}[J(0)-a_3]a_1+\frac{1}{2}a_2a_3+\frac{a_4}{2\rho}e^{-\rho\gamma}\right), \quad (18)$$

and

$$I_2=2\pi\left(\frac{1}{2}[J(0)-a_3]a_1^2+\frac{1}{2}a_2^2a_3+\frac{a_4}{4\rho^3}e^{-\rho\gamma}[7+6\gamma\rho]\right). \quad (19)$$

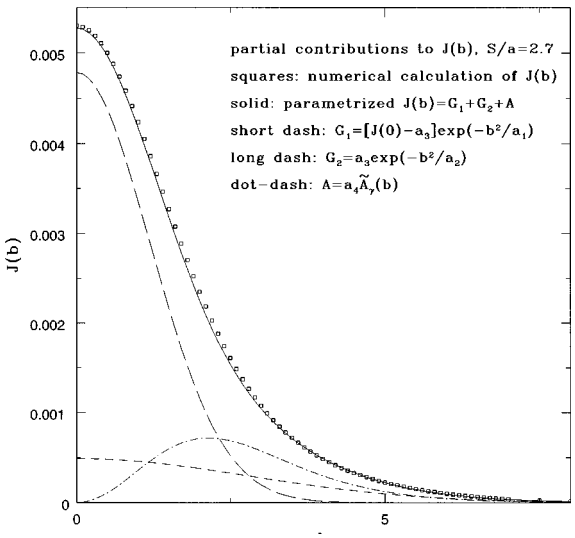

FIG. 1. Profile function $J(b)$ of the model of the stochastic vacuum for $S/a=2.7$. The squares represent the exact values [1], and the solid line represents the parametrized $J(b)$ given by Eq. (10) with partial contributions called G_1, G_2, and A.

As shown before [1,2], these expressions, which are important for the evaluation of the observables, can be conveniently parametrized as functions of S/a, leading to the forms

$$I_0=0.006\,532(S/a)^{2.791} \quad (20)$$

and

$$K=\frac{1}{2}\frac{I_2}{I_0}=2.030+0.3293(S/a)^{2.126}. \quad (21)$$

The evaluation of the amplitude through Eqs. (5) and (6) requires the integration formula

$$\int_0^\infty J_0(\beta u)\frac{e^{-\rho\sqrt{\gamma^2+u^2}}}{\sqrt{\gamma^2+u^2}}u\,du=\frac{e^{-\gamma\sqrt{\rho^2+\beta^2}}}{\sqrt{\rho^2+\beta^2}}, \quad (22)$$

and then we obtain

$$I(t)=2\pi[\tfrac{1}{2}[J(0)-a_3]a_1e^{-a^2|t|a_1/4}+\tfrac{1}{2}a_3a_2e^{-a^2|t|a_2/4}+a_4A_\gamma(t)], \quad (23)$$

where

$$A_\gamma(t)=\int_0^\infty\tilde{A}_\gamma(b)J_0(ba\sqrt{|t|})b\,db=\frac{e^{-\gamma\sqrt{\rho^2+a^2|t|}}}{\sqrt{\rho^2+a^2|t|}}-e^{\gamma\rho}\frac{e^{-\gamma\sqrt{4\rho^2+a^2|t|}}}{\sqrt{4\rho^2+a^2|t|}}. \quad (24)$$

The difference between the two terms in this expression accounts for a zero in the imaginary amplitude. With the physical value $a=0.32$ fm, the dimensionless combination $a^2|t|$ takes the reference value $a^2|t|=1$ for $|t|=0.38$ GeV^2. For

large $|t|$ (for $a^2|t| \gg 1$) the largest contributions to the amplitude $I(t)$ come from the last term, with

$$I(t) \to 2\pi a_4 \frac{e^{-\gamma\sqrt{a^2|t|}}}{\sqrt{a^2|t|}} \times \left[(1-e^{\gamma\rho}) - \frac{\gamma\rho^2}{2\sqrt{a^2|t|}} (1-4e^{\gamma\rho}) + \cdots \right], \quad (25)$$

and we observe that for large $|t|$ the amplitude is negative ($\gamma\rho$ is larger than 1). For small $|t|$ the behavior is

$$I(t) \approx 2\pi \left\{ \frac{1}{2}[J(0)-a_3]a_1 e^{-a^2|t|a_1/4} + \frac{1}{2} a_3 a_2 e^{-a^2|t|a_2/4} + a_4 \frac{e^{-\rho\gamma}}{2\rho} \times \left[1 - \left(\frac{3\gamma}{4\rho} + \frac{7}{8\rho^2} \right) a^2|t| + \ldots \right] \right\}, \quad (26)$$

where the last two terms are small compared to the first, so that the amplitude has the typical exponential behavior. However, we remark that the amplitude is not of the simple form $T(s,|t|) = T(s,0)e^{-B|t|/2}$, and the slope B must be evaluated through Eqs. (7), (18), (19). For $t=0$ we have $I_0 = I(0)$ consistently with Eq. (18).

The results obtained with MSV are correctly related to experimental data at $t=0$ (total cross section and slope), leading to the determination of the QCD parameters [1,2]. However, the predictions for the differential cross sections beyond the small values of $|t|$ are not correct, mainly because the MSV profiles put the zeros of the imaginary amplitudes at too large values of $|t|$. In the next section we introduce empirical modifications in the parameters in order to reproduce the data in the full $|t|$ range.

III. AMPLITUDES AND PROFILE FUNCTIONS FROM THE EXPERIMENTAL DATA

Using the same form of parametrization suggested by MSV, we construct the dimensionless amplitude

$$T_{\rm exp}(s,t) = 4\sqrt{\pi} s [i\mathcal{I}(t) + \mathcal{R}(t)] \quad (27)$$

directly from the experimental data (hereafter, expressions such as experimental amplitude, experimental profile, and so on will be used for quantities obtained directly from the data). The imaginary and real parts of the amplitude are parametrized using the forms

$$\mathcal{I}(t) = \alpha_1 e^{-\beta_1|t|} + \alpha_2 e^{-\beta_2|t|} + \lambda 2\rho e^{\rho\gamma} A_\gamma(t) \quad (28)$$

and

$$\mathcal{R}(t) = \lambda' 2\rho e^{\rho\gamma'} A_{\gamma'}(t) + \alpha_1' e^{-\beta_1'|t|}, \quad (29)$$

where $\rho = 3\pi/8$ and where we have grouped factors $2\rho e^{\rho\gamma} A_\gamma(t)$ in order to have $2\rho e^{\rho\gamma} A_\gamma(0) = 1$. We use eight parameters for each energy (here we do not count α_1' and β_1' which are the same for all energies, as explained below).

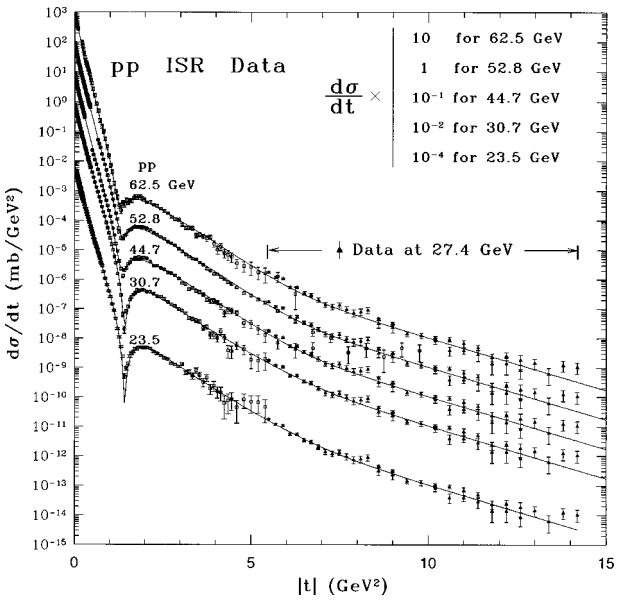

FIG. 2. Results of fittings of elastic differential cross sections through Eqs. (28) and (29) at ISR energies. Curves and data are conveniently separated in the figure through multiplication by the factors that are shown in the upper corner. The large $|t|$ data measured at 27 GeV that are drawn together with all angular distributions are described by the last term of the real amplitude in Eq. (29).

The use of $A_\gamma(t)$ in the real part, which is inspired in the MSV form for the imaginary part, has a more convenient structure, compared to simple exponentials, to fill the dip left by the zero of the imaginary part. On the other hand, the simple exponential term $\alpha_1' \exp(-\beta_1'|t|)$ was included in the real part specifically to describe the large $|t|$ ($5 < |t| < 15$ GeV^2) data [11] at 27 GeV, which is assumed to be universal for all ISR energies. This term is not present in our description of the data at 546 and 1800 GeV, where large $|t|$ values have not been measured.

We use as experimental inputs for pp scattering at ISR energies and for $p\bar{p}$ at 546 and 1800 GeV the ratio of the forward real to imaginary parts of the amplitude, $\mathcal{R}(0)/\mathcal{I}(0) \equiv \bar{\rho}$, the slope at $t=0$,

$$B = \frac{d}{dt}\left(\ln \frac{d\sigma}{dt} \right)\Big|_{t=0} = 2\frac{\mathcal{R}(0)\mathcal{R}'(0) + \mathcal{I}(0)\mathcal{I}'(0)}{\mathcal{R}^2(0) + \mathcal{I}^2(0)}, \quad (30)$$

and the total cross section determined through the optical theorem,

$$\sigma^T = 4\sqrt{\pi}\mathcal{I}(0). \quad (31)$$

After this information is introduced, the remaining parameters are determined by fitting $|\mathcal{R}(t) + i\mathcal{I}(t)|^2$ to the experimental data for $d\sigma/dt$. The results of fittings at the ISR energies and at 546 and 1800 GeV are shown in Figs. 2 and 3.

The parameters present a very regular energy dependence, as shown in Table II and Fig. 4. However, it is difficult to

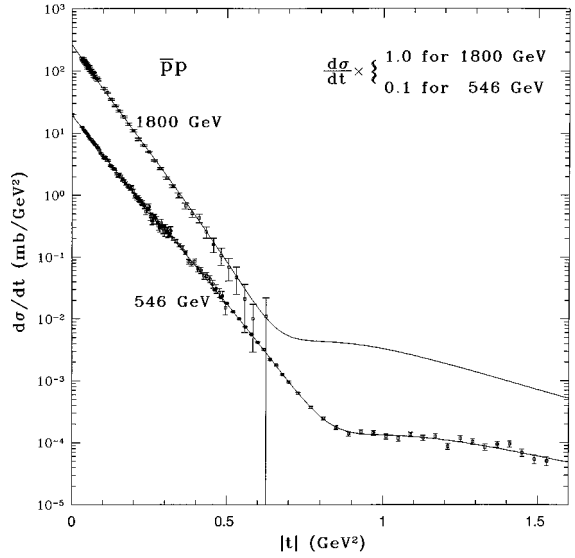

FIG. 3. Same as in Fig. 2, for 546 and 1800 GeV.

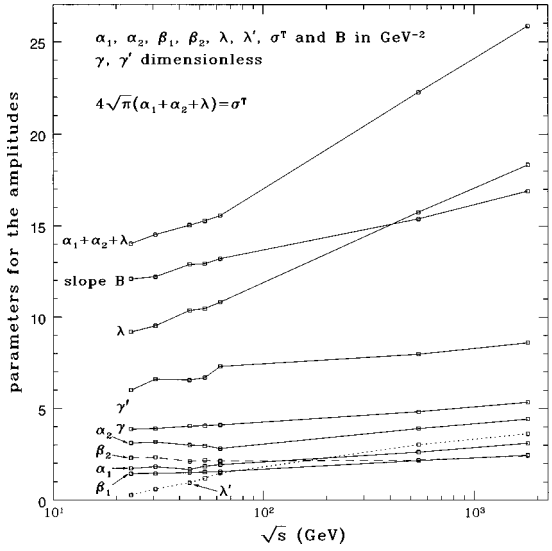

FIG. 4. Parameters of the fittings through Eqs. (28) and (29) at ISR energies, and at 546 and 1800 GeV. The energy dependence of the total cross section σ^T and the slope B obtained from the parameters are also shown.

write parametrized analytical dependences for the parameters as functions of $\sqrt{s}$ because the expressions given by Eqs. (28) and (29) are very sensitive to the values of the parameters, requiring accuracy of at least three decimals to reproduce correctly the data if we require smoothness in the variation with the energy. If each energy is considered separately, and allowing for the experimental errors in the data, the parameters are fixed typically within 1% at the energies for which the data are more accurate (e.g., 52.8 GeV).

The imaginary and real parts of the experimental scattering amplitude $T_{\rm exp}(s,t)$ are shown in Figs. 5 and 6, respectively. The figures show remarkable regularities in the energy dependence, with an interesting similarity in the behavior of all curves as functions of $|t|$. The real parts grow with the energy faster than the imaginary parts, so that even after multiplication by $1/s$ the real parts still have magnitudes which increase with s (note the inverted ordering of the curves in the two figures). At all investigated energies the imaginary amplitudes present only one zero as functions of $|t|$, with a regular displacement of the zeros towards the origin as the energy increases (shrinking of the diffraction peak). The prediction of a second zero in the imaginary part by Borrely, Soffer, and Wu [5] for very high energies (above 10 TeV) is very far for the range of our analysis. Depending on the sign given to the last term in Eq. (29), the real amplitude may present one (for negative sign) or two zeros (case of positive sign). This last term practically does not interfere with the first part, as its contribution is only important in the tail of the distribution, and thus the fitting does not determine its sign. The first zeros of the real parts are distributed in a rather small range of $|t|$ values, closer to the origin compared to the zeros of the imaginary parts. The displacement of the zeros with the energy is shown in Fig. 7 (only the first zeros of the real parts are shown).

Unfortunately the data for $d\sigma/dt$ at 1800 GeV do not go beyond $|t|=0.6$ GeV^2, and the positions of the zeros and the large $|t|$ behavior cannot be extracted from the data. Actually, Figs. 5, 6, and 7 only give (extrapolated) guesses for the quantities related to this energy.

Data at large $|t|$ (up to 15 GeV^2) obtained [11] only at 27 GeV seem to offer a natural extrapolation for the angular distribution at all ISR energies, as shown in Fig. 2. This tail is described by the term $\alpha_1' e^{-\beta_1'|t|}$ in the real part in Eq. (29), with small values for α_1' and β_1', which hardly influence the determination of the other parameters. Thus we have a term specific for the energy-independent tail, which has been included in the curves of Fig. 2. The large $|t|$ tail in $d\sigma/dt$ has

TABLE II. Values of parameters for Eqs. (28) and (29). α_1, β_1, α_2, β_2, λ, and λ' are in GeV^{-2}. γ, γ' are dimensionless. $\alpha_1'=0.0031$ GeV^{-2} and $\beta_1'=0.41$ GeV^{-2} are the same for all ISR energies.

$\sqrt{s}$	α_1	β_1	α_2	β_2	λ	λ'	γ	γ'	χ^2
23.5	1.7298	1.4390	3.1091	2.2949	9.1850	0.2774	3.8620	6.00	1.16
30.7	1.8224	1.4502	3.1649	2.3299	9.5467	0.6073	3.9000	6.600	1.21
44.7	1.6699	1.5025	3.0000	2.1086	10.3650	0.9354	4.0311	6.550	4.28
52.8	1.8500	1.5287	2.9600	2.1753	10.4630	1.1913	4.0540	6.685	3.22
62.5	1.9272	1.5529	2.8081	2.1337	10.8201	1.4747	4.0924	7.300	1.75
546	2.6174	2.1539	3.9061	2.1813	15.7463	3.0270	4.8190	7.970	1.23
1800	3.1036	2.4526	4.4246	2.4253	18.3315	3.6204	5.3450	8.600	2.00

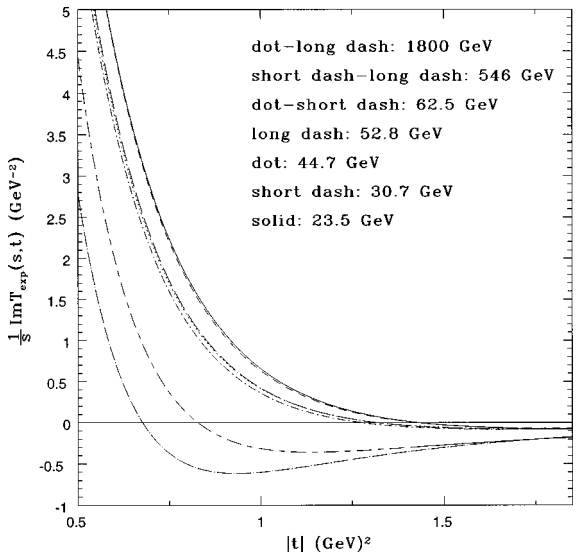

FIG. 5. Imaginary part of the experimental scattering amplitude at the ISR energies and at 546 and 1800 GeV, divided by s.

been parametrized [13] in the form $0.09/t^8$, and to have an expression with this behavior and that at the same time can be used for all $|t|$, we may modify Eq. (29) to have the form

$$\mathcal{R}(t)=\lambda' 2\rho e^{\rho\gamma'}A_{\gamma'}(t)+\alpha_1''[1-e^{-\beta_1''/(a^2|t|)^4}]. \quad (32)$$

We discuss this representation in the next section.

To obtain the profile functions from the experimental data, we invert the Fourier-Bessel transform

$$\mathcal{R}(t)+i\mathcal{I}(t)=2\pi\int_0^\infty [\mathcal{K}(\tilde{b})+i\mathcal{J}(\tilde{b})]J_0(\tilde{b}\sqrt{|t|})\tilde{b}d\tilde{b}, \quad (33)$$

where $\tilde{b}\equiv ab$ (here $\tilde{b}$ is in Fermi or GeV^{-1} units). We then obtain the desired (dimensionless) imaginary and real parts of the profile function

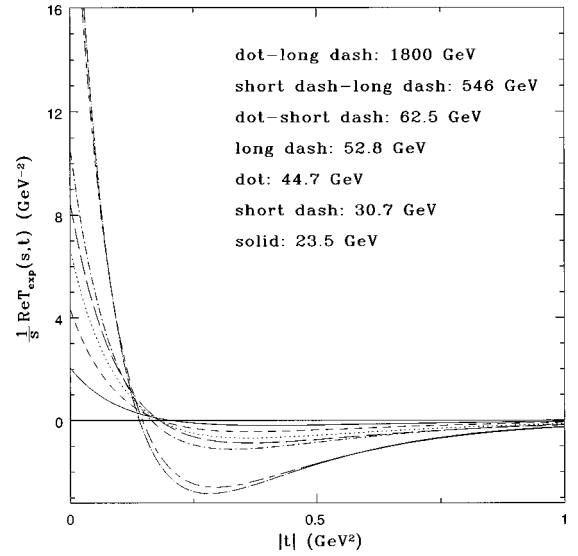

FIG. 6. Same as in Fig. 5, but for the real part of the amplitude.

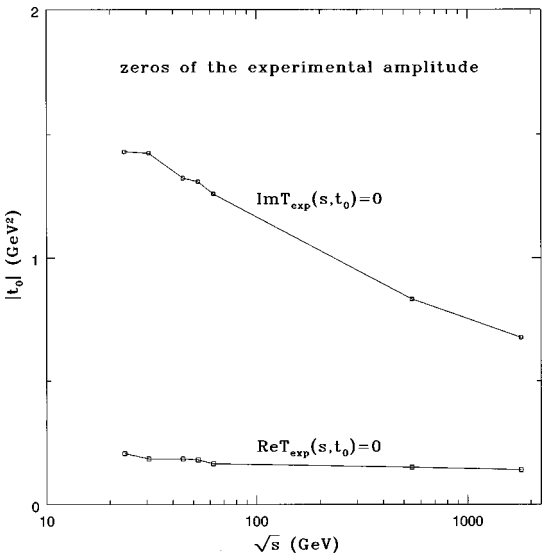

FIG. 7. Locations of the zeros of the imaginary and real parts of the amplitude as functions of the energy.

$$\mathcal{J}(\tilde{b})=\frac{1}{4\pi}\left[\frac{\alpha_1}{\beta_1}e^{-\tilde{b}^2/4\beta_1}+\frac{\alpha_2}{\beta_2}e^{-\tilde{b}^2/4\beta_2}+4\frac{\lambda\rho}{a^2}e^{\rho\gamma}\tilde{A}_\gamma(\tilde{b}/a)\right] \quad (34)$$

and

$$\mathcal{K}(\tilde{b})=\frac{1}{4\pi}\left[4\frac{\lambda'\rho}{a^2}e^{\rho\gamma'}\tilde{A}_{\gamma'}(\tilde{b}/a)+\frac{\alpha_1'}{\beta_1'}e^{-\tilde{b}^2/4\beta_1'}\right]. \quad (35)$$

To follow the same notation used for the profile function of MSV [see Eq. (10) and recall that in MSV we have only the imaginary part of the amplitude] we must introduce a numerical factor

$$J_{\mathrm{exp}}(\tilde{b})=\frac{4\sqrt{\pi}}{[\langle g^2FF\rangle a^4]^2}\mathcal{J}(\tilde{b}), \quad (36)$$

with $4\sqrt{\pi}/[\langle g^2FF\rangle a^4]^2=2.02\times10^{-2}$.

Given the experimental profiles $\mathcal{K}(\tilde{b})$ and $\mathcal{J}(\tilde{b})$, we can now write convenient expressions for comparison between the experimental quantities and those of MSV. We define the moments of the experimental profile functions corresponding to the imaginary part of the scattering amplitude,

$$\mathcal{I}_k\equiv 2\pi\int_0^\infty \tilde{b}^k\mathcal{J}(\tilde{b})\tilde{b}d\tilde{b}, \quad (37)$$

and to the real part

$$\mathcal{R}_k\equiv 2\pi\int_0^\infty \tilde{b}^k\mathcal{K}(\tilde{b})\tilde{b}d\tilde{b}, \quad (38)$$

which depend only on $\sqrt{s}$. The moments can be evaluated analytically, and are given by expressions similar to Eqs. (18) and (19).

Including the real part, the expression for the slope parameter at $t=0$ in terms of the moments $\mathcal{R}_k$ and $\mathcal{I}_k$ is

$$B_{\rm exp}=\frac{\mathcal{R}_0\mathcal{R}_2+\mathcal{I}_0\mathcal{I}_2}{2(\mathcal{R}_0^2+\mathcal{I}_0^2)}=\frac{\overline{\rho}\mathcal{R}_2+\mathcal{I}_2}{2(1+\overline{\rho}^2)\mathcal{I}_0}, \tag{39}$$

where $\mathcal{R}_0/\mathcal{I}_0=\overline{\rho}$. The maximum error in $B_{\rm exp}$ caused by the suppression of the real part contribution is about 2% at 1800 GeV and less than 1% at the ISR energies.

In order to compare experimental quantities with those of MSV, we must have a correspondence between the experimental values of $\sqrt{s}$ and the MSV values of S/a for the proton radius [1,2]. We then require that

$$I_0(S/a)=\mathcal{I}_0(s)\frac{4\sqrt{\pi}}{[\langle g^2FF\rangle a^4]^2a^2}, \tag{40}$$

which means that the evaluated total cross sections must be the same. The solutions of this equation can be written in a simple parametrized form

$$S/a=2.1848+0.1623\ln\sqrt{s}. \tag{41}$$

According to the phenomenology of the application of MSV to pp and $\overline{p}p$ scattering [1,2], the experimental and MSV values of σ^T and B are fixed to be the same for each one of the two input energies (541, 1800 GeV). This fixes the two fundamental QCD quantities (gluon condensate and correlation length) and the values of the effective proton radius at each of these two energies. Then the MSV and experimental calculations of I_2 (and obviously the ratio I_2/I_0 that gives the slope B) agree within 1 to 2% accuracy at all energies. This is the basis of the success of the MSV calculation of total cross sections and slopes.

It is important to compare our results with those obtained by Carvalho and Menon (CM) [4], who parametrized the scattering amplitude (here rewritten according to our notation) using a sum of exponentials in the form

$$F(s,t)=-\mu(s)\sum_{j=1}^{2}\alpha_j e^{-\beta_j|t|}+i\sum_{j=1}^{n}\alpha_j e^{-\beta_j|t|}, \tag{42}$$

where

$$\mu(s)=-\frac{\overline{\rho}(s)}{(\alpha_1+\alpha_2)}\sum_{j=1}^{n}\alpha_j, \tag{43}$$

with coefficients obtained by fitting $d\sigma/dt=\pi|F(s,t)|^2$ to the pp experimental data at the ISR energies ($n=4-6$, depending on the energy). The corresponding dimensionless profile functions are

$$\mathcal{K}_{\rm CM}(\tilde{b})=-\frac{\mu(s)}{2}\sum_{j=1}^{2}\frac{\alpha_j}{\beta_j}e^{-\tilde{b}^2/4\beta_j} \tag{44}$$

for the real part, and

$$\mathcal{J}_{\rm CM}(\tilde{b})=\frac{1}{2}\sum_{j=1}^{n}\frac{\alpha_j}{\beta_j}e^{-\tilde{b}^2/4\beta_j} \tag{45}$$

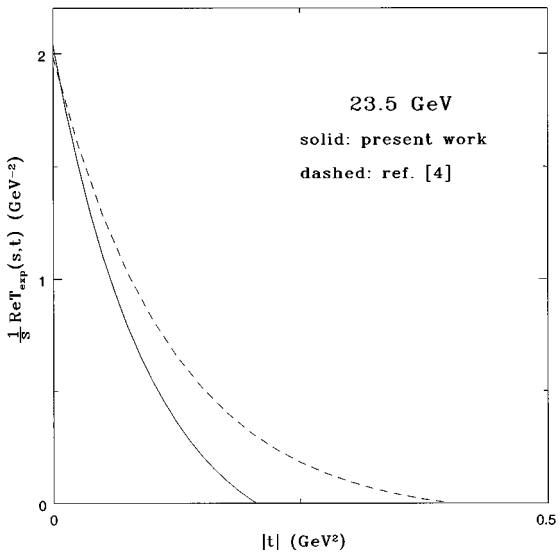

FIG. 8. Comparison of the real parts of the experimental amplitudes at 23.5 GeV obtained in our work (solid curve) and by Carvalho and Menon (CM) [4] (dashed curve).

for the imaginary part. Comparison with our formulas is given by the correspondence of values

$$\mathcal{K}_{\rm CM}(\tilde{b})=2\sqrt{\pi}\mathcal{K}(\tilde{b}),\quad \mathcal{J}_{\rm CM}(\tilde{b})=2\sqrt{\pi}\mathcal{J}(\tilde{b}). \tag{46}$$

Our imaginary amplitudes $\mathrm{Im}[T_{\rm exp}(s,t)]/4\sqrt{\pi}s=\mathcal{I}(t)$ and the values of $\sqrt{\pi}\,\mathrm{Im}[F(s,t)]$ obtained by Carvalho and Menon are very similar for all ISR energies. The Fourier tranforms $\mathcal{J}(\tilde{b})$ and $\mathcal{J}_{\rm CM}(\tilde{b})$, however, coincide only between $b=0$ and $b=2$. On the other hand, the real amplitudes $\mathrm{Re}[T_{\rm exp}(s,t)]/4\sqrt{\pi}s=\mathcal{R}(t)$ and $\sqrt{\pi}\,\mathrm{Re}[F(s,t)]$ differ substantially for all values of $|t|$, except at $|t|=0$ where they coincide (within the experimental error), because of the input experimental value for $\overline{\rho}$. The comparison of the real parts obtained in the two works is illustrated in Fig. 8 for the amplitudes and in Fig. 9 for the profile functions.

In spite of these differences in the real parts, the two parametrizations are equivalent with respect to the description of the data at each separate energy. However, our results are distinguished by the very regular energy dependence of the parameters. This regularity, which is important for interpolations and extrapolations, is true up to the highest energies 540 and 1800 GeV and also includes the angular distribution at large $|t|$ measured at 27 GeV.

IV. COMMENTS AND CONCLUSIONS

The application of MSV to high-energy scattering leads to a good description of the observables determined by the forward amplitude (σ^T and B), but the predictions for the differential cross sections for large $|t|$ are not correct, mainly because the MSV profiles put the zero of the imaginary amplitude at values of $|t|$ that are systematically higher than those required by the data. The model gives a dynamical, QCD-based framework to evaluate the forward amplitude in the eikonal formalism, and in its present formulation does

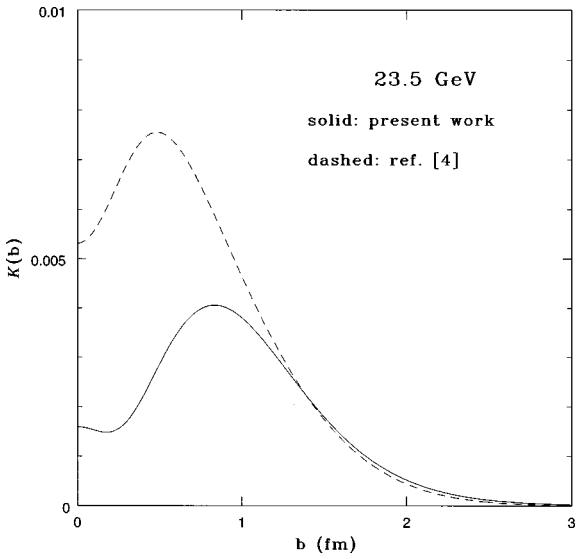

FIG. 9. Same as Fig. 8, but for the real parts of profile functions, with the correspondence between profiles given in Eq. (46). In our representation (solid line) the value of the profile function at $b=0$ is fully given by the second term of the amplitude, that only refers to the tail.

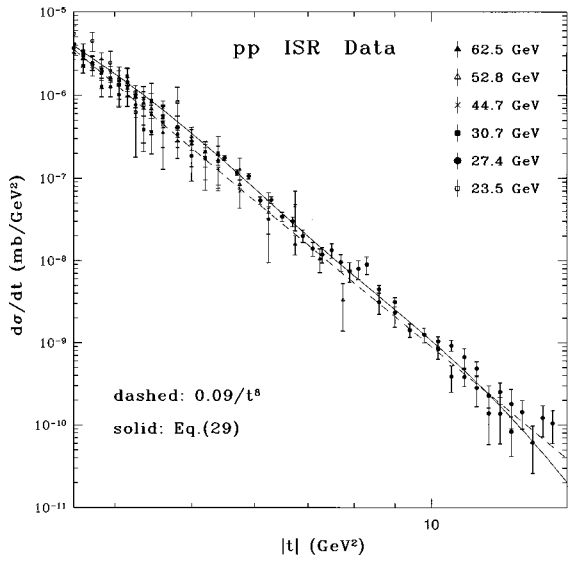

FIG. 10. Differential cross section for large $|t|$ values. Comparison between the parametrization given by Eqs. (28) and (29), and the $1/|t|^8$ dependence [13] produced by Eq. (32).

not intend to describe elastic scattering at all $|t|$, that would require the inclusion of a real part in the amplitude and changes in the imaginary part. In the present work, starting from the analytical forms of the profile function and amplitude suggested by the model, we investigate the modifications needed to fit all elastic-scattering data of the pp and $\bar{p}p$ systems at high energies. Values are obtained for the parameters and we believe that the results are made rather unique through the effort to obtain a smooth energy dependence. The chosen form respects the properties of the profile function and is such that the two-dimensional Fourier transform can be written analytically. The existence of a zero in the imaginary amplitude is a common feature of both the MSV calculation and the experimental data, and the measured differential cross section requires that this zero be filled up with the contribution from the real part. We thus must add a real part to the MSV amplitude.

In our parametrization the 27 GeV tail ($5 \lesssim |t| \lesssim 15$ GeV^2) is specifically described by a term in the real part. The large $|t|$ amplitude is probably dominated by perturbative contributions, such as triple gluon exchange, which is real and can account for the observed $0.09/t^8$ behavior [13], although it is surprising that there is no energy dependence. Figure 10 shows the comparison between the exponential form used in Eq. (29) and the power behavior produced by Eq. (32). In this last case the values of the parameters are $\alpha_1''=0.001$ GeV^{-2} and $\beta_1''=23650$. Both forms describe well the data.

In Table II we have chosen a positive sign for the tail term added to the real part, although it could also be negative, the different choices only requiring a slight adjustment of parameters. A positive sign in this term causes a second zero in the real amplitude occurring at $|t| \approx 2$ GeV^2, but there appears no dip because the imaginary part is large in this region. The first zero of the real amplitude occurs at very small $|t|$ for either sign of the tail term. The roles of the real and imaginary parts of the amplitude, and separately of the real term for the tail, considering its two possible signs, are shown in Fig. 11.

Figure 12 shows the profile functions obtained from MSV and from the fitting to the data. A general fact is that the experimental profile functions are lower for small b and higher for intermediate b values, compared to the MSV shapes. Due to the product $\tilde{b}J(\tilde{b})$ that appears in the two-

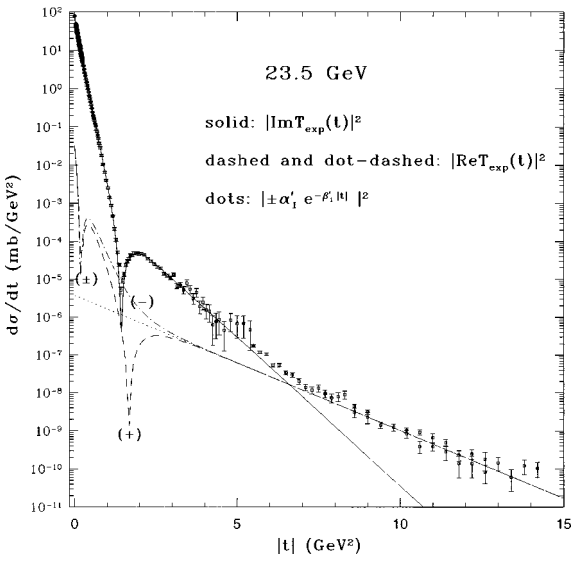

FIG. 11. Separate roles of $|\mathrm{Im}\,T|^2$ and $|\mathrm{Re}\,T|^2$ at 23.5 GeV. The dip in the data at about 1.5 GeV^2 is due to a zero in Im T. The real part is positive at $t=0$, becomes negative at small $|t|$ and fills partially the dip in $d\sigma/dt$. The dotted line represents the squared tail term alone. If this term is positive, it causes a second zero when added to Re T, as shown by the $(+)$ line. In the $(-)$ line the tail is negative and no second zero exists.

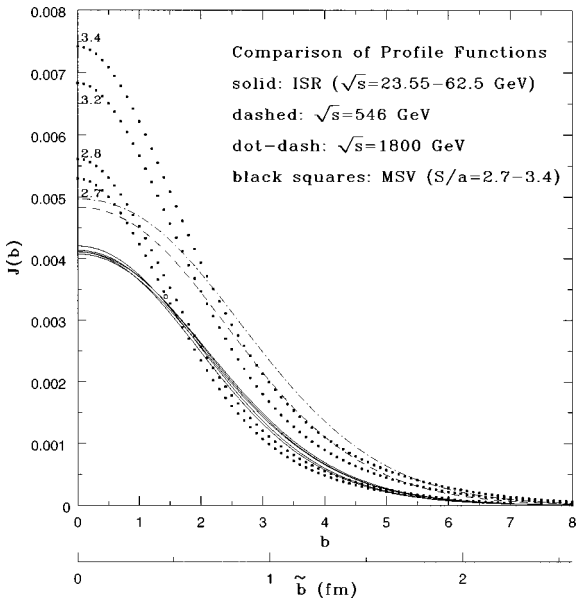

FIG. 12. Comparison of values of $J(b)$ from experimental data and from MSV, for corresponding values of $\sqrt{s}$ and S/a according to the requirement established by Eq. (40).

dimensional Fourier transform, the region about $\tilde{b} \simeq 0$ has little physical significance. It is then more instructive to examine the forms of the product $\tilde{b}J(\tilde{b})$, as shown in Fig. 13. We remark that in this figure corresponding MSV and experimental profiles have the same area (the moments I_0 fix the total cross section). In a plot of $b^3 J(b)$ the corresponding profiles also have the same areas, since the MSV moments I_2 yield the correct slopes.

The present development of the MSV formalism applied to hadron-hadron scattering [1] is restricted to the lowest order nonvanishing contribution, which is quadratic in the gluonic correlator, and has been shown to be sufficient for

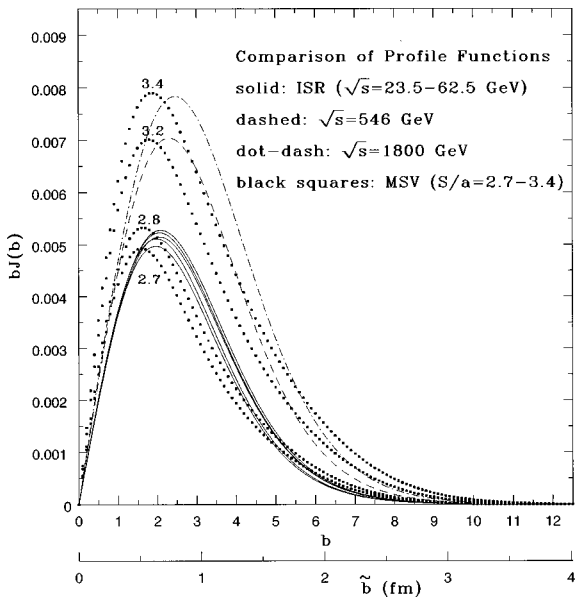

FIG. 13. Same as in Fig. 12, but for $bJ(b)$.

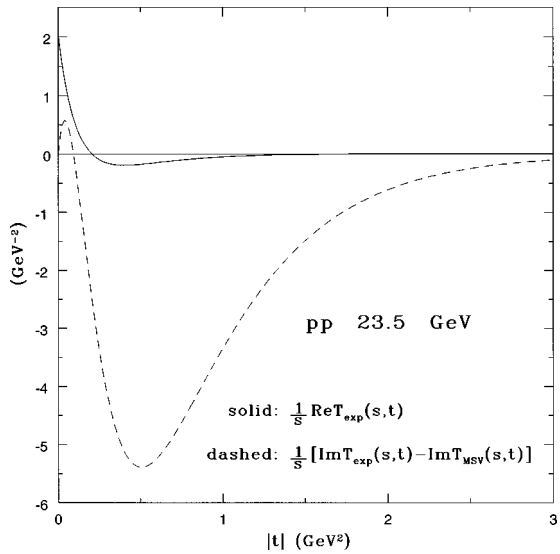

FIG. 14. The real part of the amplitude and difference between the imaginary parts of the amplitude obtained from the experiments and from the MSV calculation, all at 23.5 GeV.

the evaluation of total cross sections and slope parameters. The resulting amplitude is purely imaginary, and the ratio of the real to the imaginary parts of the elastic scattering amplitude can only be described if we go one further order in the contributions of the correlator. On the other hand, we have verified that changes in the form of the correlation functions $D(z^2/a^2)$ and $D_1(z^2/a^2)$, that enter the definition of the correlator, and reasonable changes of the hadron wave function, have little effect on the results.

In addition to these considerations, which concern mainly the nonperturbative nature of the model, we must also take perturbative contributions into account. To the MSV calculation, which represents single Pomeron exchange, we may add terms with mixed Pomeron and multiple gluon exchanges, which modify the imaginary and real parts, and may add three gluon exchange (purely real) for the tail [13].

In Fig. 14 we plot the difference at 23.5 GeV between the experimental and MSV imaginary parts of the amplitude $T(s,t)$

$$\frac{1}{s}[\mathrm{Im}\, T_{\mathrm{exp}}(s,t) - \mathrm{Im}\, T_{\mathrm{MSV}}(s,t)],$$

which illustrates the contribution to be added to the MSV result for the imaginary part, which must be mostly negative, peaked at about $|t| = 0.5$ GeV^2. In the same figure we plot the real part that is extracted from the data. We observe that, except for a small range of very small $|t|$ values, the corrections to the imaginary part must be much larger than the values of the real amplitude. The situation is similar for the other energies. These remarks may guide future theoretical developments.

Figure 15 shows the real parts of the profile function for all energies of our investigation. We observe a very regular energy dependence. The quantity $\tilde{A}_{\gamma'}(\tilde{b}/a)$ in Eq. (35) is zero for $b=0$, so that the value at the origin is due only to

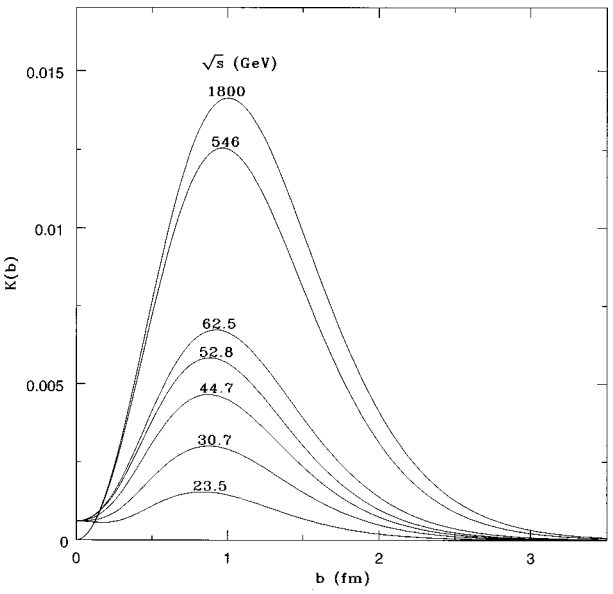

FIG. 15. The real part $\mathcal{K}(b)$ of the experimental profile functions for all ISR energies, 546 GeV and 1800 GeV.

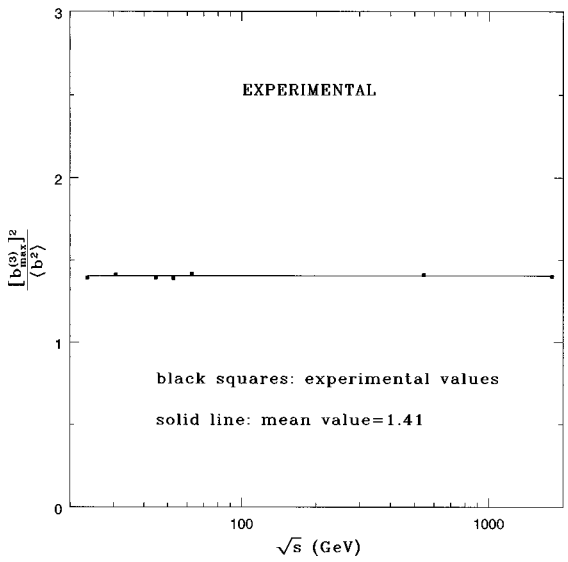

FIG. 16. Values of the experimental ratio $[b^{(3)}_{\max}]^2/\langle b^2\rangle$ (black squares) and its mean value (line).

the tail term, being the same for all ISR energies, and not included at 5540 and 1800 GeV.

Now we comment on the relation between observables in high-energy scattering and the hadronic sizes. The geometrically extended character of the nonperturbative QCD interaction determines the phenomenological properties of the observables, which are fixed by the sizes and global structures of the colliding systems. These features have led to models of a geometric nature for high-energy scattering [6], that give a natural account of the relations between total cross sections and slopes of the diffractive peaks of different hadronic systems. A geometrical relation of this sort is seen if we write Eq. (8) in the form

$$B=\frac{1}{2}\,\frac{\int d\tilde{b}\tilde{b}^2[\tilde{b}J(\tilde{b})]}{\int d\tilde{b}[\tilde{b}J(\tilde{b})]}=\frac{1}{2}\langle\tilde{b}^2\rangle \tag{47}$$

and interpret $\langle\tilde{b}^2\rangle$ as the average value of the square of the impact parameter taking $\tilde{b}J(\tilde{b})$ as weight function. There is an interesting relation between this average value $\langle\tilde{b}^2\rangle$ and the square of the value $\tilde{b}^{(3)}_{\rm m}$ of the impact parameter at the peak of the function $\tilde{b}^3J(\tilde{b})$ that appears in the upper integrand of Eq. (47). We have verified that the ratio $[\tilde{b}^{(3)}_{\rm m}]^2/\langle\tilde{b}^2\rangle$ of these two quantities extracted from the data is a constant in a wide energy range, as shown in Fig. 16. In the case of a pure Gaussian profile (i.e., an amplitude with a single exponential in t) this ratio is 1.5. This property helps us to define an effective hadronic radius, related to $\tilde{b}^{(3)}_{\rm m}$, in terms of a measurable quantity. It is remarkable, and may be of practical importance for the determination of slopes, that the position $\tilde{b}^{(3)}_{\rm m}$ of the peak is not dramatically sensitive to the details of the amplitude close to $t=0$.

A convenient parametrization of the experimental values of $\tilde{b}^{(3)}_{\max}$ is

$$\tilde{b}^{(3)}_{\max}=1.0119+0.0433\ln\sqrt{s}, \tag{48}$$

and with the correspondence between S/a and $\sqrt{s}$ given by Eq. (41), we may also write

$$\tilde{b}^{(3)}_{\max}=0.4290+0.2668(S/a). \tag{49}$$

The quantity $\tilde{b}^{(3)}_{\max}$ (written above in Fermis, while $\sqrt{s}$ is in GeV) can be extracted from the amplitude and gives a measurement of the effective hadronic size. Equation (49) connects the effective hadronic collision radius with the radius of the transverse wave function. As the energy varies from 23 to 1800 GeV, $\tilde{b}^{(3)}_{\max}$ varies from 1.15 to 1.34 fm. We obtain for $\sqrt{s}=14$ TeV the predictions $\tilde{b}^{(3)}_{\max}=1.43$ fm, $S/a=3.73$, and $B_{\rm exp}=18.76\ \ {\rm GeV}^{-2}$.

ACKNOWLEDGMENTS

The authors wish to thank M. J. Menon, P. A. Carvalho, and A. Martini for information on their work and for numerical data of experimental measurements.

[1] H. G. Dosch, E. Ferreira, and A. Krämer, Phys. Lett. B **289**, 153 (1992); **318**, 197 (1993); Phys. Rev. D **50**, 1992 (1994).
[2] E. Ferreira and F. Pereira, Phys. Rev. D **55**, 130 (1997); Phys. Lett. B **399**, 177 (1997).
[3] H. G. Dosch and M. Rueter, Phys. Lett. B **380**, 177 (1996).
[4] P. A. Carvalho and M. Menon, Phys. Rev. D **56**, 7321 (1997).
[5] C. Bourrely, J. Soffer, and T. T. Wu, Phys. Rev. D **19**, 3249 (1979); Nucl. Phys. **B247**, 15 (1984); Phys. Lett. B **252**, 287 (1990); **315**, 195 (1993).
[6] E. Ferreira and F. Pereira, Phys. Rev. D **56**, 179 (1997).
[7] Data on pp and $\tilde{p}p$ systems. (a) N. Amos *et al.*, Nucl. Phys. **B262**, 689 (1985); (b) R. Castaldi and G. Sanguinetti, Annu. Rev. Nucl. Part. Sci. **35**, 351 (1985); (c) U. Amaldi and K. R. Schubert, Nucl. Phys. **B166**, 301 (1980); (d) C. Augier *et al.*, Phys. Lett. B **316**, 448 (1993); (e) N. Amos *et al.*, *ibid.* **243**, 158 (1990); N. Amos *et al.*, *ibid.* **247**, 127 (1990); Phys. Rev. Lett. **68**, 2433 (1992).
[8] E. Nagy *et al.*, Nucl. Phys. **B150**, 221 (1979); K. R. Schubert, *Tables on Nucleon-Nucleon Scattering*, in *Numerical data and Functional Relationships in Science and Technology*, Landolt-Börnstein, New Series, Vol. I/9a (Springer-Verlag, Berlin, 1979).
[9] M. Bozzo *et al.*, Phys. Lett. **147B**, 392 (1984); M. Bozzo *et al.*, *ibid.* **147B**, 385 (1984).
[10] N. A. Amos *et al.*, Phys. Lett. B **247**, 127 (1990); see also Fermilab-FN562[E710], 1 (1991).
[11] W. Faissler *et al.*, Phys. Rev. D **23**, 33 (1981).
[12] F. Abe *et al.*, Phys. Rev. D **50**, 5550 (1994); **50**, 5518 (1994).
[13] A. Donnachie and P. V. Landshoff, Z. Phys. C **2**, 55 (1979); Nucl. Phys. **B231**, 189 (1984); Phys. Lett. B **387**, 637 (1996).